Biomaterials 225 (2019) 119501

Contents lists available at ScienceDirect

Biomaterials

journal homepage: www.elsevier.com/locate/biomaterials

Near-infrared boosted ROS responsive siRNA delivery and cancer therapy with sequentially peeled upconversion nano-onions

Yuling He[a], Shuwen Guo[b], Lina Wu[a], Pengwen Chen[a], Leyong Wang[b], Liu Ying[a,*], Ju Huangxian[a,*]

[a] State Key Laboratory of Analytical Chemistry for Life Science, School of Chemistry and Chemical Engineering, Nanjing University, Nanjing, 210023, China
[b] Key Laboratory of Mesoscopic Chemistry of MOE and Collaborative Innovation Center of Chemistry for Life Sciences School of Chemistry and Chemical Engineering, Nanjing University, Nanjing, 210023, China

HIGHLIGHTS

- Sequentially responsive UCNOs are proposed with stacked polymer coating layers for gene therapy.
- Inner layer PEI-RB boosts ROS generation intracellularly in response to external NIR stimuli.
- Middle layer PEI-SeSe completely decomposes in response to ROS for high efficient siRNA release.
- Outer layer HA decomposes in tumor microenvironment to provide siRNA delivery specificity.

ARTICLE INFO

Keywords:
Upconversion nano-onions (UCNOs)
Sequential response
Reactive oxygen species (ROS)
siRNA delivery

ABSTRACT

RNA interference (RNAi) therapy has become an appealing approach for cancer treatment, while the specificity and efficiency of controlled small interference RNA (siRNA) release remain challenging due to the heterogeneity of tumor environment. Herein, upconversion nano-onions (UCNOs) with stacked polymer coating layers are constructed to decompose sequentially in response to extracellular environment and NIR stimulation. The UCNOs (UCNPs-PEIRB-PEISeSe/siRNA-R8-HA) are composed of upconversion nanoparticles (UCNPs) core functionalized with inner coating layer of photosensitizer rose bengal (RB) conjugated PEI 600, middle coating layer of singlet oxygen ($^1O_2$) sensitive diselenide linked PEI 600 with therapeutic siRNA loading and cell-penetrating peptide R8 modification, and outer coating layer of negatively charged hyaluronic acid (HA). HA prevents siRNA leakage during delivery process and specifically targets tumor cells with overexpressed CD44 membrane receptors, and digested by cell secreted hyaluronidase (HAase). Upon the subsequent irradiation at 808 nm, UCNPs core generates emissions around 540 nm, which activate RB to boost ROS generation for complete PEI-SeSe decompose. The NIR boosted decompose of UCNOs induces a fast and efficient siRNA release, which effectively improves the gene silencing efficiency *in vitro* and suppresses tumor growth *in vivo*. The proposed sequentially responsive UCNOs have promising potential application in precision medicine.

1. Introduction

Using exogenous small interference RNA (siRNA) to selectively silence gene expression and inhibit protein transcription, gene interference therapy is becoming a promising precise approach for disease therapy [1,2]. Many stimuli-responsive nanoparticle based siRNA delivery systems have been developed in recent years, which utilize external (including light [3,4], temperature [5], magnetic field [6,7], etc) or internal stimulus (including pH [8,9], small molecule [10,11], etc) for controlled siRNA release [11,12],. Along with the extensive exploration of nanosystems as siRNA delivery vehicles, the main challenge still remains as the lack of efficiency for delivering a sufficient payload into the tumor cells [13–15]. A major limitation of the single stimuli responsive delivery system lies in the lack of conjoint spatial and temporal control, which attenuates the therapeutic effect and results in an off-target effect [16,17]. Therefore, sequential responsive delivery systems, which incorporate multiple external and internal triggers to function in a serial manner, have been develop to facilitate the specific transport of the nanocarrier to the desired destination and subsequent release of protected cargos [18].

* Corresponding authors.
E-mail addresses: yingliu@nju.edu.cn (Y. Liu), hxju@nju.edu.cn (H. Ju).

https://doi.org/10.1016/j.biomaterials.2019.119501
Received 13 June 2019; Received in revised form 30 August 2019; Accepted 18 September 2019
Available online 20 September 2019
0142-9612/

Reactive oxygen species (ROS) are highly reactive molecules or free radicals. The intracellular signalling ROS, including H_2O_2, superoxide anions ($O_2^{\cdot-}$) and hydroxyl radicals ($HO^{\cdot}$) [19,20], are capable of oxidizing boronic ester/acids, sulfides, thioketals, selenium, tellurium, proline oligomers to trigger nanocarrier intracellular disassembly and corresponding drug release [21]. The nanocarriers containing C–Se and Se–Se bonds with relatively low bond energies [22] are especially interested recently due to their response to mild oxidase under physiological relevant conditions [23,24]. However, the extracellular matrix is also oxidative as a result of ROS overproduction and oxidative stress in human body [25,26], which can damage the ROS responsive nanovehicle during delivery process and lead to early release of siRNA. On the other hand, endogenous ROS levels in cancer cells are usually not high enough and unevenly distributed due to tumor heterogeneity, therefore result in low efficiencies for cleaving the ROS-responsive caging groups and intracellular drug release [27,28]. Considering the complexity of physiological environment and tumor micro-environment, an ideal nanoparticle based delivery system for fragile siRNA should not only keep the payloads from any passive leakage in the delivery process but also readily unload the cargoes once entering into the target cells [29].

Engineering the shell-stacked nanoparticles with the sequential stimuli-responsive core-shell separations is an ideal approach [30,31]. Here we designed upconversion nano-onions (UCNOs) by combining upconversion nanoparticles (UCNPs) core with three stacked shell layers from inside out: photosensitizer rose bengal (RB) conjugated PEI (PEI-RB), ROS responsive diselenide bonds connected PEI (PEI-SeSe) with cell-penetrating peptide R8 modification, and hyaluronic acid (HA) (Scheme 1a). The negatively charged outer layer HA not only prolonged blood circulation [32], prevented UCNOs degradation during delivery process, but also provided spatial control of UCNOs transport by specifically targeting tumor cell via cell membrane receptor CD44 [33]. In tumor microenvironment, the outer layer HA underwent enzymatic degradation first by hyaluronidase (HAase), which is excessively secreted by tumor cells to expose the positively charged R8 and prompt cell internalization and lysosome escape processes.

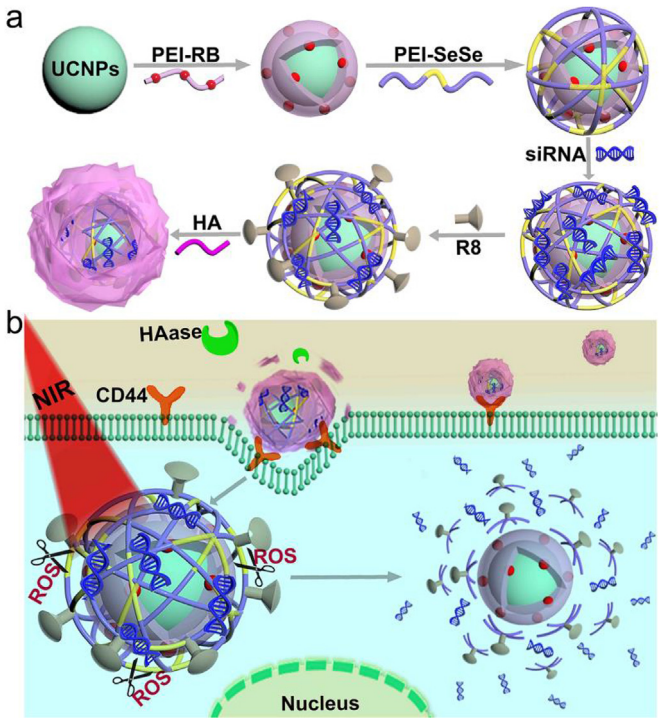

Scheme 1. Schematic illustration of (a) synthesis of UCNOs (UCNP-PEIRB-PEISeSe/siRNA-R8-HA), and (b) sequential responsive decompose of UCNOs and NIR boosted intracellular siRNA release and therapy.

Therapeutic siRNA was electrostatically adsorbed on the middle layer PEI-SeSe, and NIR irradiation provided temporal control of siRNA release by 525 nm and 540 nm light emitted from UCNPs core to activate RB in the inner coating layer PEI-RB for boosting ROS generation to completely decompose middle layer PEI-SeSe as well as siRNA release (Scheme 1b). The sequentially stripping of UCNOs not only improves delivery specificity and avoids off-target toxicities by effectively avoiding siRNA leakage during delivery process, but also prompts the gene therapy efficiency by the boosted ROS generation, therefore provides a universal strategy for efficient NIR-assisted gene therapy.

2. Materials and methods

2.1. Materials and reagents

1-Ethyl-(3-dimethyllaminopropyl) carbodiie hydrochlide (EDC·HCl), N-hydroxysuccinimide (NHS), chloropropionic acid, nitrosonium tetrafluoroborate ($NOBF_4$), selenium powder, diethy pyrocarbonate (DEPC), glutathion (GSH), bromohexanoic acid, sodium dodecyl sulfate (SDS), cyanine5 NHS ester (Cy5-NHS), maleic anhydride and N, N-dicyclohexylcarbodiimide (DCC) were purchased from J &K Chemical Co (Beijing, China). Rose Bengal (RB), branched poly (ethylenimine) (PEI, 0.6 kDa, 25 kDa), oleic acid (OA), 1-octadecene (ODE), and 1,3-diphenyl-isobenzofuran (DPBF) were purchased from Sigma-Aldrich (USA). LysoTracker red was obtained from Invitrogen Life Technologies (USA). Dulbecco's modified eagle's medium (DMEM), 4, 6-diamidino-2-phenylindole (DAPI), trypsin, penicillin streptomycin, 3-[4,5-dimethylthiazol-2-yl]-2,5-diphenyltetra- zoliumbromide (MTT), fetal bovine serum (FBS), phosphate buffered saline (PBS, pH 7.4), 6 X siRNA loading buffer, Annexin V-FITC apoptosis detection kit were purchased from KeyGEN BioTECH (Nanjing, China). Cell-penetrating peptide R8 was obtained from Shanghai Qiaoyao Biotechnology Co. Ltd (Shanghai, China). Human hepatocellular carcinoma (HepG2) cells and African green monkey kidney fibroblast (COS7) cells were purchased from Cell Bank of Chinese academy of Sciences. Hyaluronic acid (HA, 30 kDa), hyaluronidase (HAase), yttrium chloride (YCl_3, 99%), ytterbium chloride ($YbCl_3$, 99%), erbium chloride ($ErCl_3$, 99%), sodium hydroxide (NaOH, 96%), ammonium fluoride (NH_4F, 98%) and agarose were ordered from Alfa Aesar (Shanghai, China). RNA extraction kit, PrimeScript RT reagent kit and SYBR premix EX Taq kit were obtained from Takara (Dalian, China). PLK1 ELISA kit was obtained from Jin Yibai Biological Technology (Shanghai, China). Therapeutic siRNA targeting PLK1 mRNA sequence (sense strand: 5′-AUAUUCGACUUUG GUUGCCTT-3′, antisense strand: 5′-GGCAACCAAAGUCGAAUAUTT-3′) and FAM fluorescein-labelled nontherapeutic siRNA sequence (FAM-siRNA) (sense strand: 5′-FAM-UUCUCCGAACGUGUCACGUTT-3′, antisense strand: 5′-ACGUGACACGUUCGGAGAATT-3′) were designed and synthesized by GenePharma Co. Ltd (Suzhou, China). All other reagents and solvents were of analytical grade and used directly.

2.2. Apparatus

UV–Vis absorption spectra were recorded on a Nanodrop-2000C UV–Vis spectrophotometer (Nanodrop, USA). Fourier-transform infrared (FT-IR) spectra were recorded on a Nicolet 6700 spectrophotometer (Nicolet, Canada). Thermogravimetric analysis (TGA) was performed on a Setaram TGA 92 instrument (Setaram, France). Upconversion emission spectra were measured with a ZolixScan ZLX-UPL spectrometer (Beijing, China) with an external continuous-wave laser (808 nm) as the excitation light source. Transmission electron microscopic (TEM) micrographs were acquired with JEM-2100 transmission electron microscope (JEOL Ltd., Japan), and confocal fluorescence images were acquired on TCS SP5 confocal laser scanning microscope (Leica, Germany). Flow cytometric analysis was performed on Coulter FC-500 flow cytometer (Beckman-Coulter, USA). MTT and ELISA assays were performed on Hitachi/Roche System Cobas 6000

(Bio-Rad, USA). Real-time PCR was carried out with CFX96 touch real-time PCR detection system (Bio-Rad, USA). Zeta potential and dynamic light scattering (DLS) were measured with Zetasizer Nano-ZS (Malvern Instruments, UK) and ZetaPlus 90 Plus/BI-MAS (Brook haven, USA), respectively.

2.3. Synthesis of PEI-RB, PEI-SeSe and PEI-SeSe(Cy5)

Rose bengal RB (1 mmol) was reacted with 6-bromohexanoic acid (1.2 mmol) in acetone/water (7:3, v/v) at 75 °C for 24 h. After acetone was removed under vacuum, the remained solution was extracted with water-ethyl acetate to collect RB-COOH and freeze-dried. The obtained RB-COOH was characterized by mass spectrum (MS, m/z 1109, $m/z+1$ 1110 found). After activating RB-COOH (30 mg, 0.03 mmol) with EDC (3 mg, 0.015 mmol) and NHS (3 mg 0.065 mmol) in DMF (20 mL) for 2 h, PEI 600 (20 mg, 0.03 mmol) was added and vigorously stirred for 24 h. The as-prepared PEI-RB was dialyzed (molecular weight cut-off, 1 kDa), freeze-dried, and characterized by FT-IR (Fig. S1).

Selenium powder (0.40 g, 5 mmol) and $NaBH_4$ (0.38 g, 10 mmol) were mixed in a three-necked round bottom flask under nitrogen protection with the subsequent addition of 15 mL cool water, and the mixture was kept stirring at 0 °C for 15min. After adding another quantity of selenium powder (0.40 g, 5 mmol), the solution was heated to 70 °C for 30 min with the subsequent addition of 3-chloropropanoic acid (1.09 g, 10 mmol, pH 8.0), the obtained mixture solution was stirred at room temperature overnight under nitrogen protection. After 4-h exposure to atmosphere, the pH of the reaction solution was adjusted to 3–4 with 1 M HCl and the formed precipitate was collected by filtration, washed with water, and dried under reduced pressure to give SeSe–COOH as a pale yellow solid (0.26 g, 17%). ^{1}H NMR ($CDCl_3$, 400 MHz, 298 K) δ (ppm): 12.73 (s), 3.05 (t, 2H, J = 8.0 Hz), 2.71 (t, 2H, J = 8.0 Hz).

Under nitrogen protection, SeSe–COOH (0.52 g, 1.7 mmol), EDC (0.80 g, 4.2 mmol) and NHS (0.48 g, 4.2 mmol) were dissolved in THF (10 mL) in a Schleck flask and stirred at room temperature overnight. After removing solvent under reduced pressure, the as-prepared activated ester was redissolved in anhydrous DMSO (1 mL) for further use. PEI 600 (0.50 g, 1 mmol) was dissolved in water, adjusted to pH 7.4 with HCl solution, freeze-dried and redissolved in anhydrous DMSO (2 mL), which was mixed with the above DMSO solution of ester, stirred for 2 days at room temperature under nitrogen protection. After dialysis and lyophilization, PEI-SeSe was obtained as yellow solid (0.62 g, 60%). ^{1}H NMR (D_2O, 400 MHz, 298 K) δ (ppm): 2.61–2.81, 2.85–3.08 ($(CH_2)_2$–SeSe–COOH), 2.45–2.61, 3.08–3.25 (PEI 600).

PEI-SeSe (100 mg) and cyanine5 NHS ester (Cy5-NHS, 1 mg) were dissolved in anhydrous DMSO (0.4 mL) under nitrogen protection and stirred for 24 h at room temperature. After dialysis and lyophilization, PEI-SeSe(Cy5) was obtained as blue solid (88 mg).

2.4. Synthesis of core-shell UCNPs: $NaYF_4$:Er,Yb@$NaYF_4$:Yb,Nd

The $NaYF_4$:Yb, Er UCNPs core was synthesized according to the previous report [34]. Briefly, YCl_3 (0.78 mmol), $YbCl_3$ (0.2 mmol), and $ErCl_3$ (0.02 mmol) were mixed with OA (6 mL) and ODE (15 mL), heated to 120 °C and stirred for 1 h to remove oxygen and water. After cooling down to room temperature, 10 mL methanol solution containing NH_4F (4 mmol) and NaOH (2.5 mmol) was added dropwise into the mixture under stirring within 15 min. The reaction solution was then heated to 90 °C for 15 min and 300 °C for 1.5 h under N_2 atmosphere. After the resultant solution was cooled to room temperature and precipitated with ethanol to get $NaYF_4$:Yb, Er nanoparticles, the nanoparticles were re-dispersed in cyclohexane for further use. For the synthesis of $NaYF_4$:Er,Yb@$NaYF_4$:Yb, Nd core-shell UCNPs, $YbCl_3$ (0.08 mmol), $NdCl_3$ (0.32 mmol), and YCl_3 (0.4 mmol) were mixed with ODE (15 mL) and OA (6 mL), heated to 120 °C, stirred for 1 h, and subsequently cooled down to 80 °C. The UCNPs core of $NaYF_4$: Yb, Er was added into the mixture and the resulting solution was heated to 90 °C to remove the cyclohexane. After adding methanol solution (10 mL) of NH_4F (4 mmol) and NaOH (2.5 mmol) at 45 °C, the solution was stirred at room temperature for 30 min and continuously stirred at 300 °C for 1 h under a nitrogen atmosphere to get the core-shell UCNPs $NaYF_4$:Er,Yb@$NaYF_4$:Yb,Nd, which were precipitated with ethanol and re-dispersed in 10 mL cyclohexane for further use. The size and surface morphology of UCNPs were characterized by TEM, and the property was characterized by fluorescence spectrometer.

2.5. Preparation of UCNPs-PEIRB-PEISeSe, UCNPs-PEISeSe and UCNPs-PEIRB-PEISeSe(Cy5)

PEI-RB was modified on the above synthesized core-shell UCNPs according to previously reported method with small optimization [35]. Briefly, 5 mL cyclohexane containing UCNPs (5 mg/mL) was mixed with 5 mL DMF solution of $NOBF_4$ (0.01 M) at room temperature, gently shaken for 0.5 h, centrifuged and re-dispersed in DMSO. Subsequently, PEI-RB (60 mg) was added into the DMSO dispersion of UCNPs (10 mL, 2.5 mg/mL), and vigorously stirred for 30 min to get the UCNPs-PEIRB after centrifugation. After discarding the supernatant with unreacted fraction and washed with DMSO, the remaining UCNPs-PEIRB was then mixed with maleic anhydride in DMSO, and stirred at room temperature overnight to obtain the carboxyl-terminated UCNPs-PEIRB-COOH. The UCNPs-PEIRB-COOH (40 mg) was activated with EDC (45 mg) and NHS (32 mg) for 4 h at room temperature, mixed with PEI-SeSe (80 mg) in DMSO, and continuously stirred for 24 h at room temperature to get the UCNPs-PEIRB-PEISeSe after centrifugation to remove unreacted fractions. The modification process was characterized with FT-IR spectrometer, the size and properties of as-prepared UCNPs-PEIRB-PEISeSe were characterized by DLS and Zeta potential measurements, respectively. UCNPs-PEIRB-PEISeSe(Cy5) was synthesized with the similar approach for quantification of PEI-SeSe layer degradation, and UCNPs-PEISeSe was also synthesized with the similar approach as negative control.

2.6. Loading of siRNA and preparation of UCNOs (UCNPs-PEIRB-PEISeSe/siRNA-R8-HA), R8-free UCNOs (UCNPs-PEIRB-PEISeSe/siRNA-HA) and RB-free UCNOs (UCNPs-PEISeSe/siRNA-R8-HA)

siRNA was loaded into UCNPs-PEIRB-PEISeSe based on electrostatic interaction. Different amounts of UCNPs-PEIRB-PEISeSe were mixed with 2 μg siRNA with series weight ratios (1/1, 2/1, 3/1, 4/1, 5/1, 6/1), incubated for 30 min at room temperature, gently mixed with 2 μL 6 X siRNA loading buffer, and applied to the agarose gel retardation assay on 0.8% of agarose gel containing 5% of goldview. The resulting free siRNA migrations were analyzed by electrophoretic mobility shift assay using imaging on Biorad ChemDoc XRS. Using the residual –NH_2 group on UCNPs-PEIRB-PEISeSe surface, carboxyl group functionalized cell-penetrating peptide R8 was covalently modified on nanoparticle surface, and the resulting positively charged UCNPs-PEIRB-PEISeSe/siRNA-R8 were packed with negatively charged HA via electrostatic interaction. The UCNPs-PEISeSe/siRNA-R8-HA and UCNPs-PEIRB-PEISeSe/siRNA-HA were prepared with the similar approach. The surface modification process was characterized by DLS and zeta potential measurements.

To verify serum stability of the siRNA loaded UCNOs, UCNOs (UCNPs-PEIRB-PEISeSe/siRNA-R8-HA) and UCNOs without HA (UCNPs-PEIRB-PEISeSe/siRNA-R8), were treated with fetal blood serum (FBS, 10%, 30%), and the sizes and zeta potentials of nanoparticles were measured. Furthermore, 30 μL UCNPs-PEIRB-PEISeSe/siRNA-R8-HA and UCNPs-PEIRB-PEISeSe/siRNA-R8 at various UCNPs-PEIRB-PEISeSe/siRNA weight ratios (5/1, 6/1, 7/1) were incubated with 0.5 mg/mL RNase at 37 °C water bath for 30 min, continuously incubated with both 0.5 mg/mL HAase and 0.5 mg/mL DEPC at 73 °C for 2 h, and 2 μL of SDS (4%) was added subsequently to extract

undegraded siRNA. Agarose gel electrophoresis assay was performed after another incubation of 30 min.

2.7. Degradation of HA and siRNA release in vitro

The degradation of HA from UCNOs was characterized with DLS and zeta potential after incubated UCNOs with 0.5 mg/mL HAase solution (pH 6.5, HEPES buffer) at 37 °C water bath over prearranged time intervals. The release profiles of siRNA were subsequently evaluated at different stimulus conditions including 0.83 W cm^{-2} 808 nm NIR laser, 0.1 mM H_2O_2, 10 mM GSH respectively, and the UV–Vis absorbance of supernatant solutions containing released siRNA were measured at 260 nm. The released siRNA band was also visualized using agarose gel retardation assay after incubating siRNA loaded UCNOs with 0.5 mg/mL HAase solution (pH 6.5, HEPES buffer) at 37 °C with subsequent 808 nm irradiation.

2.8. Cell culture

The human hepatocellular carcinoma cell (HepG2, cancer cell) and African green monkey kidney fibroblast cell (COS7, normal cell) were incubated with DMEM medium containing 10% FBS and 1% penicillin-streptomycin (10000 U/mL) at 37 °C in a humidified atmosphere containing 5% CO_2.

2.9. Intracellular delivery of UCNOs

To demonstrate the intracellular delivery specificity and efficiency, 250 nM FAM-siRNA was loaded into 0.5 mg/mL of UCNPs-PEIRB-PEISeSe-R8, UCNPs-PEIRB-PEISeSe-R8-HA and UCNPs-PEIRB-PEISeSe-HA respectively, incubated with HepG2 cells (CD44 receptor overexpression) and COS7 cells (in the absence of CD44 receptor) at 37 °C respectively for 4 h, and stained with 0.1 μg/mL DAPI for 5 min to collect CLSM images. Flow cytometry was also performed to verify the cellular uptake efficiency of UCNOs. FAM-siRNA loaded UCNPs-PEIRB-PEISeSe-R8, UCNPs-PEIRB-PEISeSe-R8-HA and UCNPs-PEIRB-PEISeSe-HA were incubated with HepG2 cells and COS7 cells respectively for 4 h, washed with PBS for three times, trypsinized, collected by centrifugation at 1000 rpm for 5 min, and re-suspended in PBS to quantify the cellular accumulation of FAM-siRNA via flow cytometer.

To further verify the internalization specificity of FAM-siRNA loaded UCNOs via the HA receptor mediated endocytosis, HepG2 cells were pretreated with 5 mg/mL HA at 37 °C for 2 h as a negative control, and continuously incubated with FAM-siRNA loaded UCNOs for another 4 h before visualizing under the confocal fluorescence microscope.

2.10. ROS detection

DPBF was served as molecule probe to detect ROS generation *in vitro*. 0.5 mg/mL UCNPs-PEIRB-PEISeSe (2 mL) was mixed with 5 mg/mL DPBF ethanol solution (20 μL), irradiated with a 808 nm laser at 0.83 W cm^{-2} for 2 h, and the absorbance of DPBF in supernatant solutions were recorded at 422 nm after 2-h incubation. The same experiment was also performed in the absence of 808-nm laser irradiation as the negative control.

The intracellular ROS generation was observed by incubating HepG2 cells with 250 μg/mL UCNOs at 37 °C for 4 h and 50 μM dihydroethidium at 37 °C for 2 h sequentially, and exposed under 808-nm laser at 0.83 W cm^{-2} for 10 min to take the CLSM florescence images. Control experiments were also performed by incubating UCNOs with HepG2 cells in the absence of 808 nm laser irradiation.

2.11. Endosomal escape of siRNA

To verify the endosomal escape of siRNA, FAM-siRNA loaded UCNOs and LysoTracker Red were colocalized in endosomal compartments. The HepG2 cells were incubated with FAM-siRNA loaded UCNOs at 37 °C for 2 h and 6 h, respectively, and stained with 75 nM LysoTracker Red for 15 min to collect CLSM images.

2.12. Feasibility and efficiency of intracellular siRNA release

To confirm the feasibility of siRNA release from UCNOs into the cytoplasm, the FAM-siRNA loaded UCNOs were incubated with HepG2 cells for 2 h. The HepG2 cells were then irradiated with 808-nm laser for 40 min (5 min interval for every 8 min of light exposure to avoid heating) and additional 2-h incubation, the UCNPs emission at 650 nm and FAM-siRNA fluorescence at 529 nm in HepG2 cells were subsequently taken by CLSM. The HepG2 cells were also incubated with FAM-siRNA loaded UCNOs in the absence of 808-nm irradiation and FAM-siRNA loaded RB free UCNOs (UCNPs-PEISeSe/FAM-siRNA-R8-HA) with 808-nm irradiation respectively as the negative controls.

The efficiency of intracellular siRNA release was explored with luciferase-encoding plasmid (EGFP) as a reporter. The EGFP loaded UCNOs were incubated with HepG2 cells for 4 h, irradiated under 808-nm laser for 40 min (5 min interval for every 8 min of light exposure to avoid heating), and continuously incubated for 44 h to observe the expression of green fluorescent protein in the HepG2 cells by CLSM. The HepG2 cells were also incubated with EGFP loaded UCNOs in the absence of 808-nm irradiation and EGFP loaded PEI (Mw 25 kDa) respectively for 48 h, and followed by detecting green fluorescent protein expression with CLSM and flow cytometry.

2.13. MTT assay

MTT assay was used to investigate the biocompatibility of UCNOs. After HepG2 cells (5000 per well) were seeded in a 96-well plate and incubated in 200 μL DMEM containing 10% FBS and 1% penicillin-streptomycin overnight, the incubation medium was replaced with 200 μL fresh DMEM containing serial concentrations of UCNOs in the cell incubator for 48 h. 20 μL MTT (5 mg/mL in PBS) was subsequently added per well, and the cells were continuously incubated for 4 h. After removing medium, 50 μL DMSO was added to dissolve the crystals precipitate, and the optical density was measured at 490 nm with a Bio-Rad microplate reader. The relative cell viability was calculated by ($A_{test}/A_{control}$) x 100%. The results were compared with same concentration PEI (25 kDa) incubated HepG2 cells, and PBS incubated HepG2 cells as negative controls. The cell viability was also measured by MTT assay after exposed under 808-nm laser irradiation for different times.

The cell proliferation upon treatment with therapeutic PLK1 siRNA loaded UCNOs and NIR-laser irradiation was also evaluated by MTT assay. Control experiments were also performed by incubating non-therapeutic siRNA loaded UCNOs with HepG2 cells with NIR-laser irradiation, PLK1 siRNA loaded RB-free UCNOs with HepG2 cells in the presence of NIR-laser irradiation, PLK1 siRNA loaded PEI (25 kDa) with HepG2 cells and PBS treated HepG2 cells respectively.

2.14. Gene silencing assay

After HepG2 cells ($5x10^5$ per well) were seeded into a 6-well plate and cultured at 37 °C for 24 h, PLK1 siRNA loaded UCNOs, PLK1 siRNA loaded RB-free UCNOs, nontherapeutic siRNA loaded UCNOs and PLK1 siRNA loaded PEI at PLK1 siRNA or nontherapeutic siRNA concentrations of 250 nM were added into the 6-well. After continuing incubation of 4 h, the cells treated with PLK1 siRNA loaded UCNOs, PLK1 siRNA loaded RB-free UCNOs and nontherapeutic siRNA loaded UCNOs were exposed under 808-nm laser at the power density of 0.83 W cm^{-2} for 40 min (5 min interval for every 8 min of light exposure to avoid heating), and continuously cultured for 44 h. RT-PCR and ELISA kit were applied to evaluate the expression levels of PLK1 mRNA and PLK1

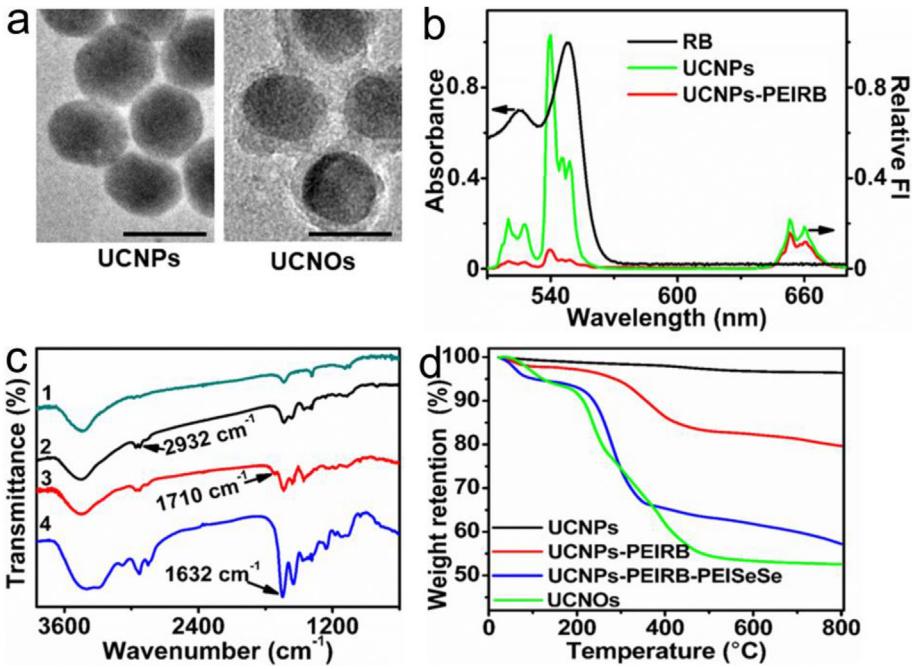

Fig. 1. Characterization of UCNPs, UCNPs-PEIRB and UCNPs-PEIRB-PEISeSe. (a) TEM image of UCNPs and UCNOs (Scale bar: 50 nm). (b) Upconversion luminescence spectra of UCNPs (green line), UCNPs-PEIRB (red line) and UV–Vis absorption spectrum of RB (black line). (c) FT-IR spectra of (1) UCNPs, (2) UCNPs-PEIRB, (3) carboxyl-functionalized UCNPs-PEIRB, and (4) UCNPs-PEIRB-PEISeSe. (d) Thermogravimetric analysis of UCNPs (black line), UCNPs-PEIRB (red line), UCNPs-PEIRB-PEISeSe (blue line) and UCNOs (green line). (For interpretation of the references to colour in this figure legend, the reader is referred to the Web version of this article.)

protein following the manufacturer's instructions respectively. The gene silencing effect of PLK1 siRNA loaded UCNOs under NIR light exposure was compared with those of same amount nontherapeutic siRNA loaded UCNOs, PLK1 siRNA loaded RB-free UCNOs, and PLK1 siRNA loaded PEI.

2.15. Cell apoptosis assay

HepG2 cells ($2x10^5$ per well) were seeded into a 6-well plate and incubated with PLK1 siRNA loaded UCNOs, PLK1 siRNA loaded RB-free UCNOs, nontherapeutic siRNA loaded UCNOs and PLK1 siRNA loaded PEI at PLK1 siRNA or siRNA concentration of 250 nM in the cell incubator for 4 h, and irradiated with 808-nm laser at 0.83 W cm^{-2} for 40 min (5 min interval for every 8 min of light exposure to avoid heating) and continuously incubated for 44 h. The cells were then collected and washed with PBS thrice and stained with the mixture of 5.0 μL Annexin V-FITC and 5.0 μL propidium iodide for 15 min and measured with flow cytometry over FL1 (Annexin V-FITC) and FL3 (PI) channels. The cell apoptosis of HepG2 cells incubated with PLK1 siRNA loaded UCNOs in the presence of NIR light irradiation were compared with nontherapeutic siRNA loaded UCNOs with NIR irradiation, PLK1 siRNA loaded RB-free UCNOs with NIR irradiation, and PLK1 siRNA loaded PEI (25 kDa).

2.16. In vivo antitumor efficiency

Pathogen-free female BALB/c nude mice (5–6 weeks) were purchased from Keygen Biotech (Nanjing, China). All experiment procedures were in accordance with the Institutional Animal Use and Care Regulations approved by the Model Animal Research Center of Nanjing University (MARC). To establish a HepG2 tumor xenograft mouse model, 1.0 $x10^6$ HepG2 cells were subcutaneously injected into the selected position of the nude mice. When the tumor volume reached 100 mm^3, the tumor-bearing mice were randomly divided into four groups with five mice in each group, and intratumorally injected with 80 μL of PBS, PLK1 siRNA loaded UCNOs, PLK1 siRNA loaded RB-free UCNOs, nontherapeutic siRNA loaded UCNOs at a dose of 1 mmol PLK1 siRNA or nontherapeutic siRNA per mouse. The tumors of mice for the groups of PLK1 siRNA loaded UCNOs, PLK1 siRNA loaded RB-free UCNOs and nontherapeutic siRNA loaded UCNOs were exposed under 808-nm laser at 0.83 W cm^{-2} for 40 min (5 min interval for every 8 min of light exposure to avoid heating). The injection and irradiation processes were repeated every other two days for six times. The tumor sizes were measured every 2 days by a caliper, and the tumor volumes were calculated as $V = (L \times W^2)/2$, where L and W are the length and width of the tumor, respectively. The mice weights were also recorded every 2 days during the therapeutic process. After 14 days of treatment, all mice were sacrificed, and the tumors were collected, weighed and photographed. Subsequently, tumors were washed by PBS thrice, fixed with 4% paraformaldehyde, embedded in paraffin, sectioned at 4 μm thickness, and stained with Hematoxylin-Eosin (H&E) and TUNEL, then viewed via CLSM.

3. Results and discussion

3.1. Preparation and characterization of UCNOs and siRNA loading

ß-$NaYF_4$ crystalline structures co-doped with Er^{3+} (2%) and Yb^{3+} (20%) were synthesized according to previously reported solvent thermal method [36,37], and coated with $NaYF_4$ shell co-doped with Nd^{3+} (40%) and Yb^{3+} (10%) to effectively harvest excitation photon at 808 nm for upconversion luminance enhancement [34]. The as-synthesized core-shell structured UCNPs ($NaYF_4$:Er,Yb@$NaYF_4$:Yb,Nd) were further reacted with $NOBF_4$ to replace surface ligand oleic acid and obtain the UCNPs that well dispersed in DMSO solution to facilitate further surface functionalization [35]. The bar-shaped UCNPs with average size of 36 ± 2.3 nm x 29 ± 1.8 nm (length x width) (Fig. 1a) demonstrated emission peaks at 525 nm and 540 nm corresponding to $^2H_{11/2} \rightarrow {}^4I_{15/2}$ and $^4S_{3/2} \rightarrow {}^4I_{15/2}$ transitions of Er^{3+}, and 650 nm corresponding to $^4F_{9/2} \rightarrow {}^4I_{15/2}$ transition of Er^{3+} (green line, Fig. 1b) [38]. RB was chosen as the photosensitizer for ROS generation due to its high photoquantum yield [39] and characteristic absorption in the range of 470–570 nm which overlapped well with the emissions of UCNPs at 525 nm and 540 nm (black line, Fig. 1b), and covalently conjugated to PEI (PEI-RB) (Fig. S1). The as-prepared PEI-RB was modified on UCNPs surface using ligand exchange reaction as the inner coating layer of UCNOs to get UCNPs-PEIRB. Compared with BF_4^- stabilized UCNPs, FT-IR spectrum of UCNPs-PEIRB showed the characteristic peak at 2932 cm^{-1} for C–H stretching vibrations of $–CH_2–$ group (line 2, Fig. 1c), and demonstrated obvious decrease of UCNPs

emission peaks at 525 nm and 540 nm due to the strong absorption of RB at corresponding wavelength range, while the emission peak at 650 nm remained unchanged (red line, Fig. 1b). The middle layer of UCNOs, PEI-SeSe was synthesized by conjugating nontoxic PEI 600 with diselenide contained cross-linker according to previously reported method [40] with 1.6 kDa of molecular mass and 1.38 of polydispersity index (PDI) confirmed by gel permeation chromatography (GPC) (Fig. S2). The surface amine groups of UCNPs-PEIRB were converted to carboxyl groups by reacting with maleic anhydride [41], and subsequently conjugated to PEI-SeSe via carbodiimide crosslinking reaction to wrap UCNPs-PEIRB with middle coating layer PEI-SeSe to get UCNPs-PEIRB-PEISeSe. The FT-IR spectrum of carboxylated UCNPs-PEIRB showed a new absorption peak at 1710 cm^{-1} for stretching vibrations of C═O for carboxyl group (line 3, Fig. 1c) [42], which disappeared for the UCNPs-PEIRB-PEISeSe along with stronger intensity of the peak at 1632 cm^{-1} for C═O stretching vibration of –CONH– [43], indicating the successful conjugation of PEI-SeSe (line 4, Fig. 1c). After the continuous surface coatings of inner layer PEI-RB and middle layer PEI-SeSe, the size of functionalized UCNPs increased to 41 ± 1.9 nm and 50 ± 2.1 nm respectively for TEM characterization, with the hydrodynamic diameter of functionalized UCNPs increased from 39 ± 1.1 nm to 46 ± 1.8 nm and 62 ± 2.6 nm respectively due to the polymer layer swelling in aqueous solution (Fig. S3 a-c) [44]. The coating of middle layer PEI-SeSe resulted little decrease for all the emission peaks at 525 nm, 540 nm and 650 nm compared with UCNPs-PEIRB (Fig. S4). Thermogravimetric analysis was performed to further confirm UCNPs surface modifications. Compared with 2% weight loss for UCNPs, the weight losses for UCNPs-PEIRB and UCNPs-PEIRB-PEISeSe were 16% and 36%, respectively (Fig. 1d), indicating the successful stacked polymer layer coatings.

siRNA was loaded to UCNPs-PEIRB-PEISeSe via electrostatic interaction, and agarose gel retardation assay was performed to optimize the weight ratio (w/w) of UCNPs-PEIRB-PEISeSe to siRNA. Free siRNA demonstrated a bright band at lower molecular mass, which became dimmer with the weight ratio of UCNPs-PEIRB-PEISeSe to siRNA increase, and disappeared at weight ratio of 5/1, indicating the complete encapsulation of siRNA in UCNPs-PEIRB-PEISeSe (Fig. 2a). The weight ratio of 6/1 was chosen for siRNA loading to guarantee the tight condensing of siRNA in the nanocarrier [45]. After the encapsulation of siRNA, the UCNPs nanocomposite was further modified with peptide R8 covalently for efficient cell uptake and endosomal escape, and subsequently coated with HA as the outer coating layer via electrostatic interaction to complete the UCNOs (UCNPs-PEIRB-PEISeSe/siRNA-R8-HA). siRNA encapsulation successfully decreased the zeta potential of UCNPs-PEIRB-PEISeSe from 36 ± 1.8 mV to 6 ± 2.1 mV, while the modification of positively charged peptide R8 increased the zeta potential to 17 ± 1.9 mV due to the abundant guanidine of R8, and the subsequent negatively charged HA coating decreased the zeta potential to −20 ± 1.4 mV due to the carboxylate group of HA (Fig. 2b). The hydrodynamic diameters of the UCNPs-PEIRB-PEISeSe slightly increased to 68 ± 2.1 nm after siRNA loading and continued to increase to 72 ± 2.4 nm after R8 conjugation and 83 ± 2.6 nm after HA wrapping from DLS measurements (Fig. 2b), while siRNA loading barely resulted size change of UCNPs-PEIRB-PEISeSe due to its lower molecular weight and corresponding small size, and R8 conjugation and HA wrapping increased particle sizes to 54 ± 2.2 nm (Fig. S3 d-e), and 60 ± 1.8 nm respectively from TEM characterization (Fig. 1a). Compared with UCNPs-PEIRB-PEISeSe, HA layer wrapping demonstrated similar intensity for all the upconversion luminance peaks (Fig. S4). The thermogravimetric analysis showed about 45% of weight loss for UCNOs (Fig. 1d, green line), further confirmed the subsequent surface modification and completion of UCNOs.

The serum stability of delivery nanovehicle is important to prolong retention time in the circulation for elevated tumor targeting [46]. The HA outer coating of UCNOs could not only specifically target the CD44 receptor on tumor cell membrane, but also avoid nonspecific protein adsorption and corresponding aggregation during systematic circulation by shielding positive surface charges [33]. To verify the serum stability, the UCNOs were exposed to PBS containing 10% and 30% fetal bovine serum (FBS) respectively, and their sizes remained at 83 ± 2.6 nm (Fig. S5a) with zeta potential remained at −20 ± 1.4 mV (Fig. S5b) over 30 h incubation. On the contrary, UCNOs in the absence of HA demonstrated continuous size increase from 72 ± 2.4 nm to 583 ± 4.3 nm in 10% FBS and 830 ± 3.8 nm in 30% FBS for DLS measurements (Fig. S5a), and the surface charge decreased from 17 ± 1.9 mV to −22 ± 2.3 mV in 10% FBS and −26 ± 2.2 mV in 30% FBS for zeta potential measurements (Fig. S5b) over incubation periods due to nonspecific protein adsorption. The UCNOs were also treated with PBS containing 20 nM H_2O_2 to mimic the oxidative extracellular environment [47], and their sizes and zeta potentials all remained unchanged during 32 h incubation (Fig. S6), demonstrating the integrity of UCNOs during delivery process. To further demonstrate the shielding effect of HA coating to protect siRNA from enzymatic degradation during delivery process, siRNA loaded UCNOs and UCNOs in the absence of HA were treated with PBS containing 0.5 mg/mL ribonuclease A (RNase A) that catalyzes RNA degradation, and the non-degradated siRNA was extracted by 4% SDS for gel electrophoresis analysis after treatment with 0.5 mg/mL diethy pyrocarbonate (DEPC) and 0.5 mg/mL HAase. The siRNA extraction bands disappeared for UCNOs in the absence of HA coating due to the penetration of RNase A into the nanocomposite and corresponding digestion of siRNA, while HA coating demonstrated satisfactory capability of protecting siRNA from RNase A degradation (Fig. S7).

3.2. Feasibility of sequential responsive siRNA release

Though facilitating the systemic circulation, the negative charge of the nanovehicle surface can impede its further penetration and internalization once accumulated in a tumor tissue [48], therefore the development of smart nanomedicine with variable size and transformable surface is a good strategy [13,49]. The stacked polymer coating layers of UCNOs sequentially responded to tumor microenvironment and external NIR irradiation to achieve controlled siRNA release. The outer shell HA was first degraded by the HAase enzyme secreted from tumor cell to expose positively charged R8 for charge-reversal of UCNOs [33], which assisted the cell internalization and endosomal escape of UCNPs-PEIRB-PEISeSe/siRNA-R8. Zeta potential was preformed to verify the HA degradation in response to 0.5 mg/mL HAase at pH 6.5, which

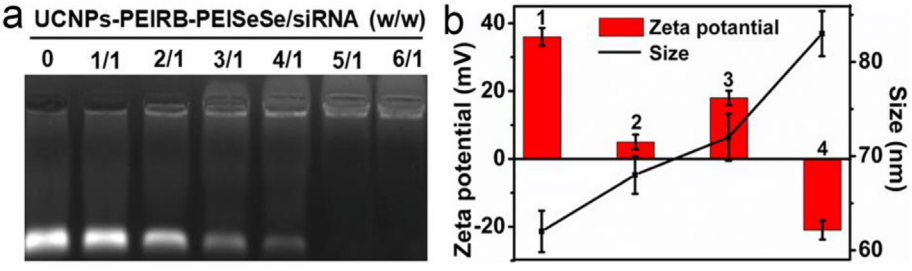

Fig. 2. Characterization of siRNA encapsulation and UCNPs-PEIRB-PEISeSe/siRNA-R8-HA. (a) Agarose gel retardation assay for UCNPs-PEIRB-PEISeSe/siRNA with various weight ratios (w/w). (b) Zeta potential and DLS analysis of (1) UCNPs-PEIRB-PEISeSe, (2) UCNPs-PEIRB-PEISeSe/siRNA, (3) UCNPs-PEIRB-PEISeSe/siRNA-R8, and (4) UCNPs-PEIRB-PEISeSe/siRNA-R8-HA. The error bars indicate means ± S.D. (n = 3).

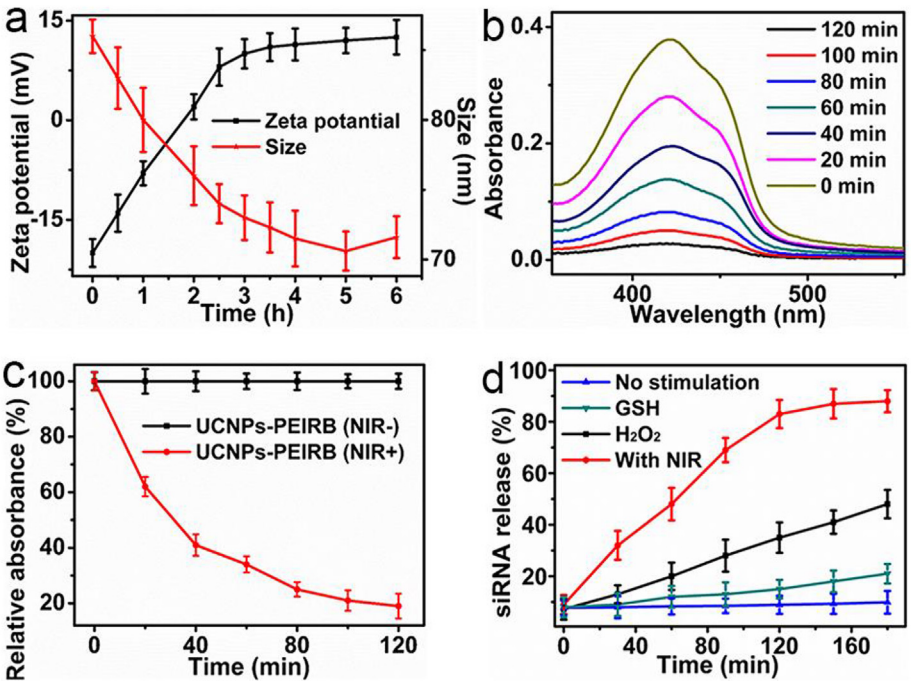

Fig. 3. Characterization of UCNOs disassembly, ROS generation and siRNA release. (a) Zeta potentials and hydrodynamic diameters of UCNOs in response to 0.5 mg/mL HAase at pH 6.5 according to time. (b) UV–Vis absorption spectra and (c) relative UV–Vis absorbance percentage of supernatant DPBF solution at 422 nm after exposing UCNPs-PEIRB under NIR irradiation for different times compared to that without irradiation. (d) siRNA release from UCNOs as a function of time in response to NIR irradiation, 100 μM H_2O_2, 10 mM GSH and in the absence of any stimulation. The error bars indicate means ± S.D. (n = 4).

continuously increased from −20 ± 1.4 mV to 12 ± 1.8 mV, indicating the gradual decompose of negatively charged HA and expose of positively charged peptide R8 (Fig. 3a). Moreover, the size of UCNOs decreased to 70 ± 2.4 nm during HA decomposing process from DLS measurements (Figs. 3a), and 52 ± 2.4 nm from TEM characterization (Fig. S8a), which were both similar to the hydrodynamic diameter and size of UCNPs-PEIRB-PEISeSe/siRNA-R8, confirming the complete degradation of HA coating layer. After taken into the cell, the stripped UCNOs (UCNPs-PEIRB-PEISeSe/siRNA-R8) was exposed to 808 nm irradiation to produce 525 nm and 540 nm emissions, which activated photosensitizer RB conjugated to inner layer PEI-RB to generate ROS for the cleavage of Se–Se bonds and the corresponding decompose of middle layer PEI-SeSe. The ROS generation upon NIR irradiation was determined by incubating UCNPs-PEIRB with 1,3-diphenylisobenzofuran (DPBF), a sensing probe which could react with ROS irreversibly to give characteristic absorption peak at 422 nm, and demonstrated a continuous intensity decrease according to time (Fig. 3b), which indicated NIR dose dependent of ROS generation and 82% absorbance decrease in 2 h (Red line, Fig. 3c). On the contrary, the incubation of UCNPs-PEIRB with DPBF at the same time in the absence of NIR light irradiation showed little absorption intensity decrease (Black line, Fig. 3c). Thermogravimetric analysis was also performed for UCNPs-PEIRB-PEISeSe after NIR light exposure, and showed a weight loss of 18% (Fig. S9), which was very similar to that of UCNPs-PEIRB, indicating the complete decompose of middle layer PEI-SeSe by photo-generated ROS. UCNPs-PEIRB-PEISeSe(Cy5) was further prepared to quantify PEI-SeSe layer degradation, which demonstrated continuous dropping of PEI-SeSe(Cy5) from UCNPs-PEIRB under NIR irradiation and reached 99.8% at 60 min (Fig. S10). TEM characterization was further performed to characterize size change after NIR irradiation (Fig. S8b), which continuously decreased to 42 ± 1.4 nm, similar to that of UCNPs-PEIRB, confirming the complete degradation of PEI-SeSe coating layer.

After treated with HAase and exposed under NIR light for different times, the supernatant solutions of siRNA encapsulated UCNOs were collected and their absorption intensities were measured at 260 nm to demonstrate the siRNA release efficiency. SiRNA demonstrated a rapid release upon 808 nm laser irradiation (Fig. S11), and the release percentage saturated at around 86% after 2 h (Fig. 3d). Compared with the previously reported siRNA release approaches from photo-decomposed polymers [50] and ROS-decomposed polymers with NIR activated photosensitizers [51,52], the combination of UCNPs and visible light activated photosensitizer guaranteed high ROS generation efficiency, and the construction of stacked thin polymer layers resulted in the effective utilization of generated ROS, which led to the complete decompose of middle layer PEI-SeSe of UCNOs and highly efficient siRNA release. The HAase treated UCNOs was also exposed to 100 μM H_2O_2 and 10 mM GSH respectively to demonstrate its response to intracellular environment [41,48], which showed a relatively slower release compared to the ROS boosted release upon NIR irradiation, and negligible release was observed from HAase treated UCNOs in the absence of any stimulation (Fig. 3d). Gel electrophoresis was also performed to further demonstrate the sequentially responsive siRNA release. siRNA loaded UCNOs treated with HAase and subsequent NIR irradiation showed bright siRNA bands at UCNPs-PEIRB-PEISeSe/siRNA weight ratio of 5/1, 6/1 and 7/1 (Fig. S12). On the contrary, siRNA loaded UCNOs demonstrated bright siRNA bands at loading positions for all UCNPs-PEIRB-PEISeSe/siRNA weight ratios in the absence of HAase pretreatment, indicating the incapability of siRNA release from UCNOs.

3.3. Internalization process of UCNOs and intracellular siRNA release

The positively charged cell-penetrating peptide R8 in UCNOs assists its endosomal escape due to the proton sponge effect of guanidine groups from R8 [53]. After the siRNA loaded UCNOs were incubated with Human hepatocellular carcinoma (HepG2) cells, the co-staining experiments were performed to identify the internalization of nanocarriers as well as endosomal escape. Endosome was stained with Lysotracker Red and siRNA was labelled with FAM (FAM-siRNA) to indicate their subcellular distributions. FAM-siRNA was localized in endosome on the same sites after 2-h incubation by the overlap of green (FAM-siRNA) and red (lysosome probe) fluorescence (Fig. S13a), indicating successful cellular internalization of siRNA loaded UCNOs. After continuing 4-h incubation, the FAM fluorescence was spread in the entire cytoplasm while weaker fluorescence of acidity dependent Lysotracker red was observed due to the raised pH of the microenvironment from endosome disruption (Fig. S13b) [54], indicating the

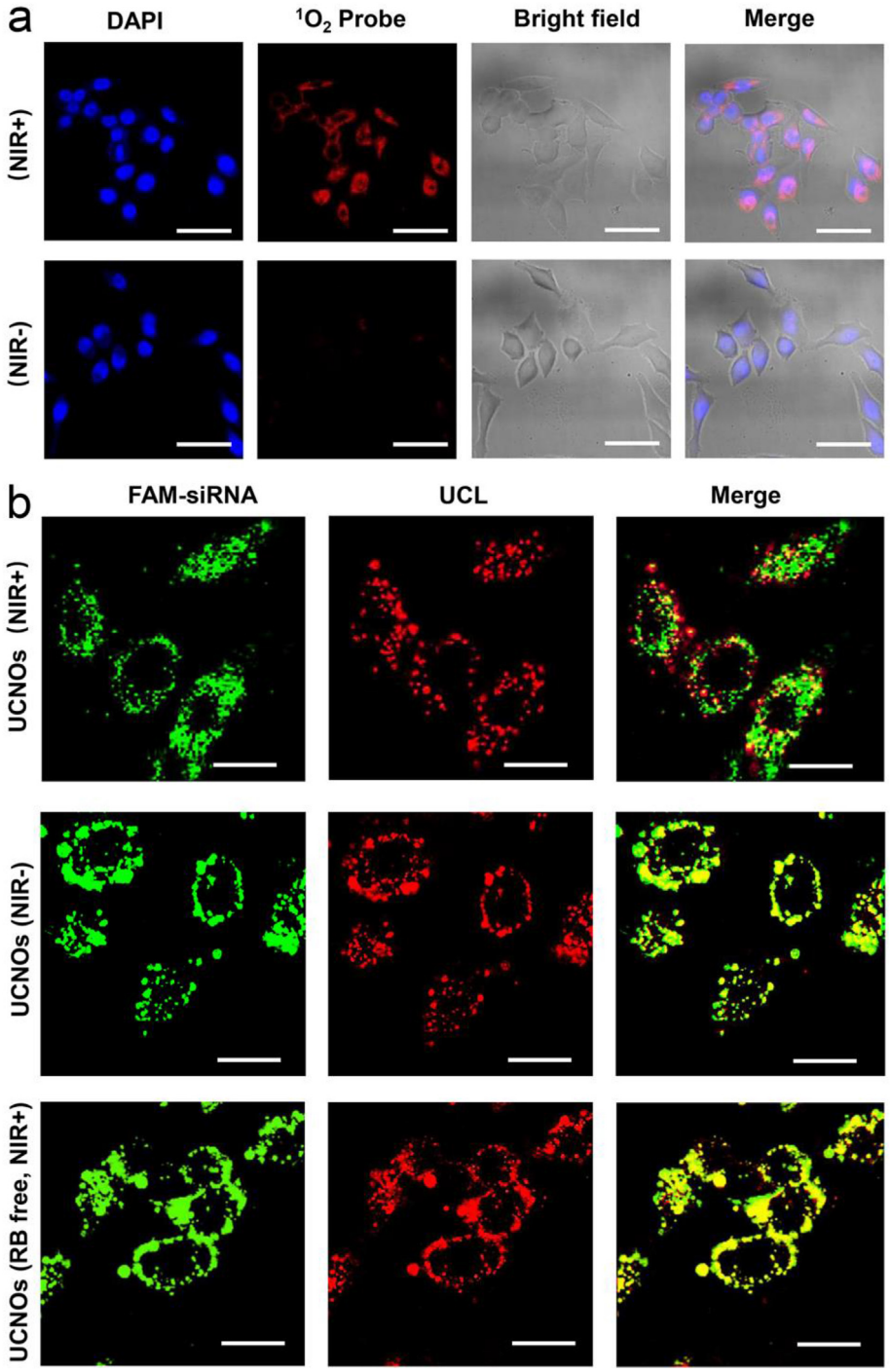

Fig. 4. ROS generation and siRNA release in HepG2 cells. Confocal microscopic images of (a) HepG2 cells treated with UCNOs and intracellular ROS detection probe in the presence and absence of NIR irradiation (Scale bar 100 μm) and (b) co-localization of UCNPs at 650 nm emission and FAM-siRNA at 529 nm emission for HepG2 cells treated with UCNOs in the presence and absence of NIR irradiation and RB free UCNOs in the presence of NIR irradiation (Scale bar 10 μm).

efficient endosomal eacape of UCNOs.

The ROS production in living cells was investigated with intracellular ROS probe dihydroethidium, which generates red emission upon ROS oxidization [55]. Strong red emission was observed for HepG2 cells incubated with UCNOs under NIR irradiation (Fig. 4a), indicating the efficient intracellular ROS generation from inner layer conjugated RB. Contrarily, little red fluorescence was observed for UCNOs incubated HepG2 cells in the absence of NIR irradiation (Fig. 4a).

To confirm the successful release of siRNA from UCNOs into the cytoplasm, FAM-siRNA loaded UCNOs was incubated with HepG2 cells for 3 h and the photoluminescence at 650 nm from UCNPs was compared with FAM emission at 529 nm. After 40 min NIR light irradiation, the green fluorescence from FAM-siRNA was obviously separated from red emission of UCNPs (Fig. 4b), demonstrated the efficient release of siRNA from UCNOs in response to NIR-generated ROS. On the contrary, the green fluorescence from siRNA and red fluorescence from UCNPs overlapped for the siRNA loaded UCNOs in the absence of NIR irradiation and the photosensitizer free UCNOs in the presence of NIR (Fig. 4b). To further verify the intracellular siRNA release efficiency, gene transfection assay was carried out by loading UCNOs with luciferase-encoding plasmid (EGFP) as a reporter in HepG2 cells, and the

expression of green fluorescent protein was observed and quantified by CLSM and flow cytometric analysis. After 40-min NIR irradiation, bright green fluorescence was observed intracellularly with 56% transfection efficiency (UCNOs, (NIR +), Fig. S14), which was better than the classic transfection agent PEI (25 kDa) with 38% transfection efficiency (PEI, Fig. S14), indicated the highly efficient EGFP release from UCNOs due to the complete decompose of middle layer PEI-SeSe. Incubation EGFP loaded UCNOs with HepG2 cells in the absence of NIR exposure also demonstrated intracellular green fluorescence to some extent due to the decompose of PEI-SeSe via intracellular ROS and H_2O_2 (UCNOs, (NIR-), Fig. S14), but the transfection efficiency (41%) was much lower compared with NIR activated transfection, which confirmed that NIR irradiation assisted ROS generation and prompted intracellular siRNA release efficiency.

To verify the HA-mediated recognition and delivery specificity, FAM-siRNA loaded UCNOs, FAM-siRNA loaded HA free UCNOs and FAM-siRNA loaded R8 free UCNOs were incubated with CD44 receptor overexpressed HepG2 cells and African green monkey kidney fibroblast (COS7) cells respectively for 4 h, and the intracellular fluorescence of FAM-siRNA were detected subsequently using CLSM. When incubated with FAM-siRNA loaded UCNOs, the HepG2 cells showed strong fluorescence, whereas little fluorescence signal was observed from COS7 cells that do not express CD44 receptor on cell membrane (Fig. 5a). In addition, HepG2 and COS7 cells demonstrated similar fluorescence intensities after 4-h incubation with FAM-siRNA loaded HA-free UCNOs. Both cells demonstrated very low fluorescence with FAM-siRNA loaded R8-free UCNOs due to the inefficiency of cell internalization in the absence of R8. Flow cytometry analysis was also performed to verify the efficiency and specificity of UCNOs delivery, which demonstrated strong fluorescence intensity for FAM-siRNA loaded UCNOs incubated HepG2 cells, while similar fluorescence was observed for HA-free UCNOs incubated HepG2 cells and COS7 cells, and little fluorescence was observed for R8-free UCNOs (Fig. 5b). These results demonstrated that both HA and R8 functionalization of UCNOs promoted HepG2 cells specific internalization process. To further confirm that HA played an important role in the delivery specificity, competition experiment was performed by previously incubating excess free HA with HepG2 cells to block the CD44 receptor [33], which barely demonstrated UCNOs internalization (Fig. 5c).

The cytotoxicity of UCNOs was evaluated with standard 3-(4,5-dimethylthiazol-2-yl)-2-diphenyltetrazolium bromide (MTT) assay at a series of UCNOs concentrations for HepG2 cells, and the results were compared with gold standard polymer delivery vehicle PEI (25 kDa). Even at high concentration of 200 μg/mL of UCNOs, HepG2 cells still kept 88% viability, while the cells treated with same concentration of PEI only exhibited 29% viability (Fig. S15a). The good biocompatibility of UCNOs guaranteed its potential application in clinical intervention. Besides, 808 nm irradiation demonstrated little effect on cell viability,

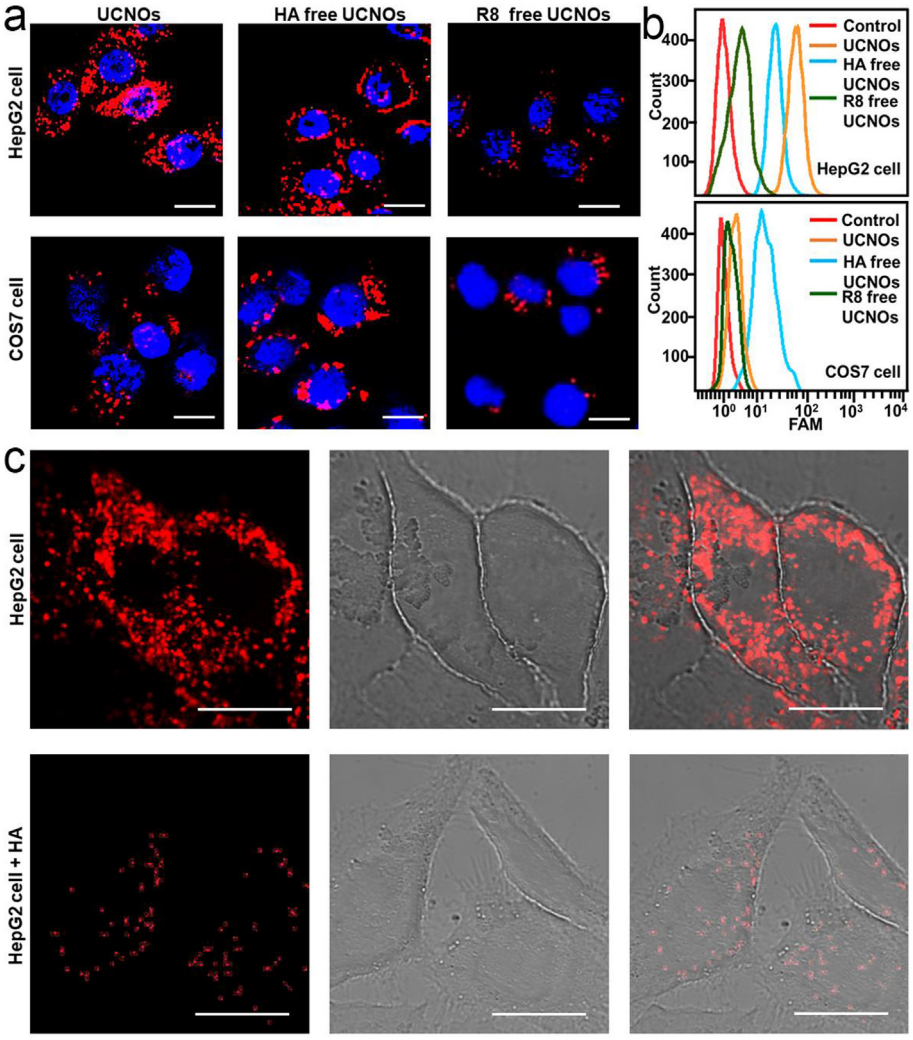

Fig. 5. The delivery specificity of UCNOs. (a) CLSM images and (b) flow cytometry analysis of FAM-siRNA loaded UCNOs, FAM-siRNA loaded HA free UCNOs and FAM-siRNA loaded R8 free UCNOs incubated with HepG2 cells and COS7 cells (Scale bar: 8 μm). (c) CLSM images of FAM-siRNA loaded UCNOs incubated with HepG2 cells and HepG2 cells pre-treated with excess free HA. (Scale bar: 5 μm).

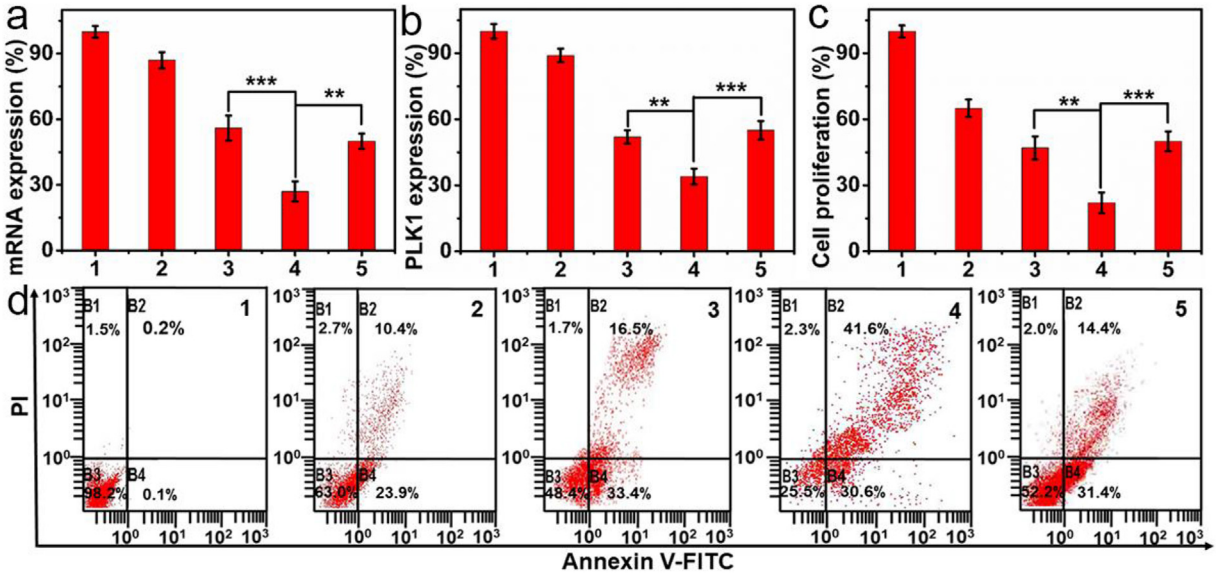

Fig. 6. Gene silencing and cell proliferation inhibition. Expression levels of (a) PLK1 mRNA detected with qRT-PCR and (b) PLK1 protein determined with ELISA. Relative HepG2 cell proliferation percentages determined with (c) MTT and (d) Annexin V-fluorescein isothiocyanate (FITC)/propidium iodide (PI) apoptotic kit. (1) Untreated HepG2 cells as control, (2) nontherapeutic siRNA loaded UCNOs in the presence of NIR irradiation, (3) PLK1 siRNA loaded RB free UCNOs in the presence of NIR irradiation, (4) PLK1 siRNA loaded UCNOs in the presence of NIR irradiation, and (5) PLK1 siRNA loaded PEI (25 kDa). $^{**}P < 0.01$, $^{***}P < 0.001$ with two-tailed student's t-test. The error bars indicate means ± S.D. ($n = 5$).

and HepG2 cell showed above 96% viability during 2 h 808 nm NIR exposure (Fig. S15b).

3.4. Gene silencing assay

The polo-like family of serine/threonine protein kinases (PLKs) has a significant impact on cell cycle regulation and proliferation, and PLK1 can promote oncogenic transformation, therefore inhibiting PLK1 expression can lead to cell cycle arrest, apoptosis, and mitotic catastrophe [56]. The HepG2 cells were incubated with PLK1 siRNA loaded UCNOs for 4 h and irradiated with 808-nm light for 40 min and continuously cultured for 48 h, and the expression levels of PLK1 mRNA and PLK1 protein were determined by qRT-PCR and enzyme-linked immunosorbent assay (ELISA) respectively. The PLK1 mRNA expression was down-regulated to 27% for the PLK1 siRNA loaded UCNOs treated HepG2 cells under NIR irradiation (column 4, Fig. 6a), which was impressively improved compared with 56% mRNA expression for PLK1 siRNA loaded RB-free UCNOs in the presence of NIR (column 3, Fig. 6a) due to the photo-boosted ROS generation which facilitated siRNA release. In addition, the UCNOs also demonstrated better inhibition effect for mRNA suppression compared with same amount PLK1 siRNA loaded PEI (25 kDa) (column 5, Fig. 6a), indicating that UCNOs could serve as excellent nanovehicles for siRNA delivery. Consistently, the inhibitions of PLK1 protein expression demonstrated similar tendency for HepG2 cells treated with UCNOs under different conditions (Fig. 6b), indicating the high gene silencing efficiency of PLK1 loaded UCNOs in the presence of NIR irradiation. The same amount of nontherapeutic siRNA loaded UCNOs were also incubated with HepG2 cells under NIR irradiation, and barely demonstrated gene silencing effect or protein expression suppression (column 2, Fig. 6a and b).

3.5. Cell apoptosis assay

MTT assay was used to verify the inhibition effect of UCNOs on HepG2 cell proliferation, and the inhibition efficiency was compared with commercial transfection reagent PEI (25 kDa). The HepG2 cells treated with PLK1 siRNA loaded UCNOs showed 22% cell proliferation percentage under NIR irradiation (column 4, Fig. 6c) due to the NIR boosted ROS generation and siRNA release, while it was 47% for the cells treated with PLK1 siRNA loaded RB-free UCNOs in the presence of NIR irradiation (column 3, Fig. 6c). The cells treated with nontherapeutic siRNA loaded UCNOs showed 65% of cell proliferation percentage under NIR irradiation (column 2, Fig. 6c), indicating the photodynamic therapy (PDT) effect of UCNOs. The cell proliferation percentage of PLK1 siRNA loaded PEI treated cell was 50% (column 5, Fig. 6c), which was not comparable to PLK1 siRNA loaded UCNOs treated cells under NIR irradiation.

Flow cytometric assay using the Annexin V-fluorescein isothiocyanate (FITC)/propidium iodide (PI) apoptotic kit showed similar phenomena. The apoptosis rate of 72.2% for PLK1 siRNA loaded UCNOs treated cells under NIR irradiation was higher compared with PLK1 siRNA loaded RB-free UCNOs treated cells in the presence of NIR irradiation (49.9%), PLK1 siRNA loaded PEI treated cells (45.8%), nontherapeutic siRNA loaded UCNOs treated cells under NIR irradiation (34.3%) (Fig. 6d). These results demonstrated the feasibility of UCNOs as a promising approach for efficient anticancer therapy.

3.6. In vivo therapeutic applicability

The *in vivo* antitumor efficacy of PLK1 siRNA loaded UCNOs were evaluated using HepG2 cell tumor-bearing nude mice. The PLK1 siRNA loaded UCNOs were intratumorally injected into the mice with subsequent NIR irradiation of 0.83 W cm^{-2} for 40 min. PBS injected mice, nontherapeutic siRNA loaded UCNOs injected mice with subsequent NIR irradiation and PLK1 siRNA loaded RB-free UCNOs injected mice in the presence of NIR irradiation were also prepared as control groups. The PLK1 siRNA loaded UCNOs presented pronounced inhibition efficiency toward tumor growth under NIR irradiation, suggesting the improved therapeutic efficiency for ROS boosted gene delivery (Fig. 7a). On the contrary, nontherapeutic siRNA loaded UCNOs in the presence of NIR irradiation and PLK1 siRNA loaded RB-free UCNOs in the presence of NIR irradiation demonstrated much lower inhibition efficiency toward tumor growth, indicating PDT alone or endogenous ROS activated PLK1 siRNA release was insufficient to achieve high therapeutic efficiency. During the 14 days of experiment period, all the mice groups did not show obvious variation in their body weights (Fig. 7b), indicating satisfactory biocompatibility and specificity of UCNOs. Mice were euthanized on day 14 when the tumor volume of

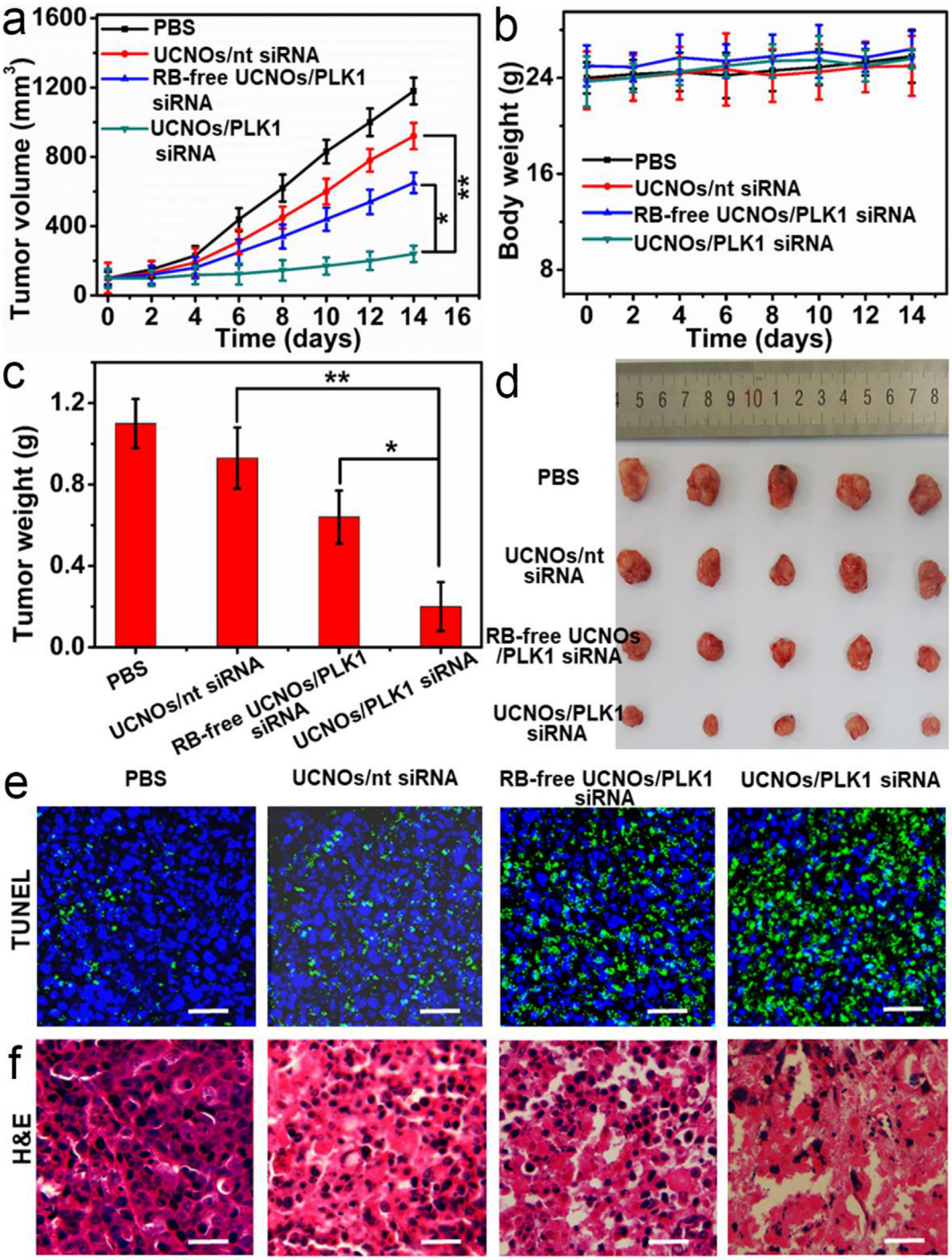

Fig. 7. *In vivo* antitumor therapy. Demonstration of therapeutic efficiency with change of (a) tumor volume, (b) body weight of mice as a function of time, (c) tumor weight, (d) representative photos, (e) TUNEL staining and (f) H&E staining of excised tumors at day 14 after treatment with PBS, nontherapeutic siRNA loaded UCNOs with NIR irradiation (UCNOs/nt siRNA), PLK1 siRNA loaded RB-free UCNOs in the presence of NIR irradiation (RB-free UCNOs/PLK1 siRNA), PLK1 siRNA loaded UCNOs in the presence of NIR irradiation (UCNOs/PLK1 siRNA) respectively. $^{*}P < 0.05$, $^{**}P < 0.01$ with two-tailed student's t-test. The error bars indicate means ± S.D. ($n = 5$) (Scale bar, 100 μm).

PBS injected group reached 1200 mm^3, and the tumors were excised and weighed, which also demonstrated the enhanced antitumor capability of PLK1 siRNA loaded UCNOs upon NIR irradiation (Fig. 7c and d). The TUNEL staining result demonstrated the largest number of apoptotic cells with strongest green fluorescence for PLK1 siRNA loaded UCNOs treated mice group with NIR irradiation (Fig. 7e). In hematoxylin and eosin (H&E) staining assays, massive cell shrinkage and nuclei absence were observed for PLK1 siRNA loaded UCNOs treated mice group with NIR irradiation, while minor nuclei absence was found in the tumor sections for nontherapeutic siRNA loaded UCNOs treated mice in the presence of NIR irradiation and PLK1 siRNA loaded RB-free UCNOs treated mice in the presence of NIR irradiation, and abundant tumor cells were found in tumor section for PBS treated mice (Fig. 7f). These tendencies were consistent with the results of cell apoptosis assays, further confirmed the enhanced therapeutic efficiency for UCNOs under NIR irradiation.

4. Conclusions

We design sequentially stripped UCNOs by constructing stacked polymer coatings around UCNPs, which provides spatial and temporal control of siRNA release and achieves highly efficient gene therapy. The UCNPs ($NaYF_4$:Er,Yb@$NaYF_4$:Yb,Nd) are functionalized with PEI-RB as the inner layer, and wrapped with ROS-responsive middle layer PEI-SeSe with subsequent loading of therapeutic siRNA via electrostatic interaction. After the surface covalent binding of R8 and outer layer HA, the UCNOs (UCNPs-PEIRB-PEISeSe/siRNA-R8- HA) are obtained. The outer layer coating HA can specifically target tumor cells and prevent siRNA leakage during delivery process, which is decomposed first at extracellular environment by the HAase enzyme secreted from tumor cells. 808-nm laser irradiation boosts ROS generation from the inner layer PEIRB, which causes complete decompose of middle layer PEI-SeSe due to oxidization of diselenide bonds, and leads to rapid release of siRNA for highly efficient gene therapy. The UCNOs show impressive inhibition for cell proliferation and tumor growth *in vivo*, therefore would be a promising platform for precise drug delivery and tumor therapy.

Data availability statement

The raw/processed data reported in this work are available upon request.

Acknowledgements

This work was financially supported by National Natural Science Foundation of China (21635005, 21605083, 21974064), National Research Foundation for Thousand Youth Talents Plan of China, Natural Science Foundation of Jiangsu Province (BK 20160644), State Key Laboratory of Analytical Chemistry for Life Science (5431ZZXM1806), Specially-appointed Professor Foundation of Jiangsu Province, and Program for Innovative Talents and Entrepreneurs of Jiangsu Province.

Appendix A. Supplementary data

Supplementary data to this article can be found online at https://doi.org/10.1016/j.biomaterials.2019.119501.

References

[1] G. Ozcan, B. Ozpolat, R.L. Coleman, A.K. Sood, G. Lopez-Berestein, Preclinical and clinical development of siRNA-based therapeutics, Adv. Drug Deliv. Rev. 87 (2015) 108–119.
[2] J.E. Zuckerman, M.E. Davis, Clinical experiences with systemically administered siRNA-based therapeutics in cancer, Nat. Rev. Drug Discov. 14 (2015) 843.
[3] L. Feng, Z. Dong, C. Liang, M. Chen, D. Tao, L. Cheng, K. Yang, Z. Liu, Iridium nanocrystals encapsulated liposomes as near-infrared light controllable nanozymes for enhanced cancer radiotherapy, Biomaterials 181 (2018) 81–91.
[4] R. Wang, L. Zhou, W. Wang, X. Li, F. Zhang, In vivo gastrointestinal drug-release monitoring through second near-infrared window fluorescent bioimaging with orally delivered microcarriers, Nat. Commun. 8 (2017) 14702.
[5] Q. Zou, M. Abbas, L. Zhao, S. Li, G. Shen, X. Yan, Biological photothermal nanodots based on self-assembly of peptide–porphyrin conjugates for antitumor therapy, J. Am. Chem. Soc. 139 (2017) 1921–1927.
[6] M.R. Mohammadi, A.V. Malkovskiy, P. Jothimuthu, K.-M. Kim, M. Parekh, M. Inayathullah, Y. Zhuge, J. Rajadas, PEG/Dextran double layer influences Fe ion release and colloidal stability of iron oxide nanoparticles, Sci. Rep. 8 (2018) 4286.
[7] H. Bi, Y. Dai, P. Yang, J. Xu, D. Yang, S. Gai, F. He, B. Liu, C. Zhong, G. An, J. Lin, Glutathione mediated size-tunable UCNPs-Pt(IV)-ZnFe2O4 nanocomposite for multiple bioimaging guided synergetic therapy, Small 14 (2018) 1703809.
[8] D.W. Malcolm, J.J. Varghese, J.E. Sorrells, C.E. Ovitt, D.S.W. Benoit, The effects of biological fluids on colloidal stability and siRNA delivery of a pH-responsive micellar nanoparticle delivery system, ACS Nano 12 (2018) 187–197.
[9] Y. He, L. Zhang, Z. Chen, Y. Liang, Y. Zhang, Y. Bai, J. Zhang, Y. Li, Enhanced chemotherapy efficacy by co-delivery of shABCG2 and doxorubicin with a pH-responsive charge-reversible layered graphene oxide nanocomplex, J. Mater. Chem. B 3 (2015) 6462–6472.
[10] J. Liu, Q. Chen, W. Zhu, X. Yi, Y. Yang, Z. Dong, Z. Liu, Nanoscale-Coordination-polymer-shelled manganese dioxide composite nanoparticles: a multistage redox/pH/H_2O_2-responsive cancer theranostic nanoplatform, Adv. Funct. Mater. 27 (2017) 1605926.
[11] N. Li, H. Yang, Z. Yu, Y. Li, W. Pan, H. Wang, B. Tang, Nuclear-targeted siRNA delivery for long-term gene silencing, Chem. Sci. 8 (2017) 2816–2822.
[12] J. Zhu, M. Qiao, Q. Wang, Y. Ye, S. Ba, J. Ma, H. Hu, X. Zhao, D. Chen, Dual-responsive polyplexes with enhanced disassembly and endosomal escape for efficient delivery of siRNA, Biomaterials 162 (2018) 47–59.
[13] J. Chen, J. Ding, Y. Wang, J. Cheng, S. Ji, X. Zhuang, X. Chen, Sequentially responsive shell-stacked nanoparticles for deep penetration into solid tumors, Adv. Mater. 29 (2017) 1701170.
[14] K. Ren, Y. Liu, J. Wu, Y. Zhang, J. Zhu, M. Yang, H. Ju, A DNA dual lock-and-key strategy for cell-subtype-specific siRNA delivery, Nat. Commun. 7 (2016) 13580.
[15] H. Cabral, Y. Matsumoto, K. Mizuno, Q. Chen, M. Murakami, M. Kimura, Y. Terada, M.R. Kano, K. Miyazono, M. Uesaka, N. Nishiyama, K. Kataoka, Accumulation of sub-100 nm polymeric micelles in poorly permeable tumours depends on size, Nat. Nanotechnol. 6 (2011) 815.
[16] J. Zhao, J. Gao, W. Xue, Z. Di, H. Xing, Y. Lu, L. Li, Upconversion luminescence-activated DNA nanodevice for ATP sensing in living cells, J. Am. Chem. Soc. 140 (2018) 578–581.
[17] Y.J. Chen, B. Groves, R.A. Muscat, G. Seelig, DNA nanotechnology from the test tube to the cell, Nat. Nanotechnol. 10 (2015) 748.
[18] N. Yoshinaga, T. Ishii, M. Naito, T. Endo, S. Uchida, H. Cabral, K. Osada, K. Kataoka, Polyplex micelles with phenylboronate/gluconamide cross-linking in the core exerting promoted gene transfection through spatiotemporal responsivity to intracellular pH and ATP concentration, J. Am. Chem. Soc. 139 (2017) 18567–18575.
[19] M. Ye, Y. Han, J. Tang, Y. Piao, X. Liu, Z. Zhou, J. Gao, J. Rao, Y. Shen, A tumor-specific cascade amplification drug release nanoparticle for overcoming multidrug resistance in cancers, Adv. Mater. 29 (2017) 1702342.
[20] G. Saravanakumar, J. Kim, W.J. Kim, Reactive-oxygen-species-responsive drug delivery systems: promises and challenges, Adv. Sci. 4 (2017) 1600124.
[21] Y. Zhang, J. Wang, J. Yu, D. Wen, A.R. Kahkoska, Y. Lu, X. Zhang, J.B. Buse, Z. Gu, Bioresponsive microneedles with a sheath structure for H_2O_2 and pH cascade-triggered insulin delivery, Small 14 (2018) 1704181.
[22] H. Xu, W. Cao, X. Zhang, Selenium-containing polymers: promising biomaterials for controlled release and enzyme mimics, Acc. Chem. Res. 46 (2013) 1647–1658.
[23] C. Sun, S. Ji, F. Li, H. Xu, Diselenide-containing hyperbranched polymer with light-induced cytotoxicity, ACS Appl. Mater. Interfaces 9 (2017) 12924–12929.
[24] V.G. Deepagan, S. Kwon, D.G. You, V.Q. Nguyen, W. Um, H. Ko, H. Lee, D.-G. Jo, Y.M. Kang, J.H. Park, In situ diselenide-crosslinked polymeric micelles for ROS-mediated anticancer drug delivery, Biomaterials 103 (2016) 56–66.
[25] D. Chen, G. Zhang, R. Li, M. Guan, X. Wang, T. Zou, Y. Zhang, C. Wang, C. Shu, H. Hong, L.J. Wan, Biodegradable, hydrogen peroxide, and glutathione dual responsive nanoparticles for potential programmable paclitaxel release, J. Am. Chem. Soc. 140 (2018) 7373–7376.
[26] Y. Li, Y. Li, W. Ji, Z. Lu, L. Liu, Y. Shi, G. Ma, X. Zhang, Positively charged polyprodrug amphiphiles with enhanced drug loading and reactive oxygen species-responsive release ability for traceable synergistic therapy, J. Am. Chem. Soc. 140 (2018) 4164–4171.
[27] M.S. Shim, Y. Xia, A reactive oxygen species (ROS)-Responsive polymer for safe, efficient, and targeted gene delivery in cancer cells, Angew. Chem. Int. Ed. 52 (2013) 6926–6929.
[28] Y. Yuan, J. Liu, B. Liu, Conjugated-polyelectrolyte-based polyprodrug: targeted and image-guided photodynamic and chemotherapy with on-demand drug release upon irradiation with a single light source, Angew. Chem. Int. Ed. 53 (2014) 7163–7168.
[29] S. Wang, G. Yu, Z. Wang, O. Jacobson, R. Tian, L.-S. Lin, F. Zhang, J. Wang, X. Chen, Hierarchical tumor microenvironment-responsive nanomedicine for programmed delivery of chemotherapeutics, Adv. Mater. 30 (2018) 1803926.
[30] W.X. Qiu, M.-K. Zhang, L.-H. Liu, F. Gao, L. Zhang, S.-Y. Li, B.-R. Xie, C. Zhang, J. Feng, X.-Z. Zhang, A self-delivery membrane system for enhanced anti-tumor therapy, Biomaterials 161 (2018) 81–94.
[31] T. Wang, D. Wang, J. Liu, B. Feng, F. Zhou, H. Zhang, L. Zhou, Q. Yin, Z. Zhang, Z. Cao, H. Yu, Y. Li, Acidity-Triggered ligand-presenting nanoparticles to overcome sequential drug delivery barriers to tumors, Nano Lett. 17 (2017) 5429–5436.
[32] Y. Lu, Q. Hu, Y. Lin, D.B. Pacardo, C. Wang, W. Sun, F.S. Ligler, M.D. Dickey, Z. Gu, Transformable liquid-metal nanomedicine, Nat. Commun. 6 (2015) 10066.
[33] W.H. Chen, G.-F. Luo, W.-X. Qiu, Q. Lei, S. Hong, S.-B. Wang, D.-W. Zheng, C.-H. Zhu, X. Zeng, J. Feng, S.-X. Cheng, X.-Z. Zhang, Programmed nanococktail for intracellular cascade reaction regulating self-synergistic tumor targeting therapy, Small 12 (2016) 733–744.
[34] B. Liu, C. Li, P. Yang, Z. Hou, J. Lin, 808-nm-Light-Excited lanthanide-doped nanoparticles: rational design, luminescence control and theranostic applications, Adv. Mater. 29 (2017) 1605434.
[35] A. Dong, X. Ye, J. Chen, Y. Kang, T. Gordon, J.M. Kikkawa, C.B. Murray, A generalized ligand-exchange strategy enabling sequential surface functionalization of colloidal nanocrystals, J. Am. Chem. Soc. 133 (2011) 998–1006.
[36] Y. Li, J. Tang, D.-X. Pan, L.-D. Sun, C. Chen, Y. Liu, Y.-F. Wang, S. Shi, C.-H. Yan, A versatile imaging and therapeutic platform based on dual-band luminescent lanthanide nanoparticles toward tumor metastasis inhibition, ACS Nano 10 (2016) 2766–2773.
[37] F. He, G. Yang, P. Yang, Y. Yu, R. Lv, C. Li, Y. Dai, S. Gai, J. Lin, A new single 808 nm NIR light-induced imaging-guided multifunctional cancer therapy platform, Adv. Funct. Mater. 25 (2015) 3966–3976.
[38] F. Ai, Q. Ju, X. Zhang, X. Chen, F. Wang, G. Zhu, A core-shell-shell nanoplatform upconverting near-infrared light at 808 nm for luminescence imaging and photodynamic therapy of cancer, Sci. Rep. 5 (2015) 10785.

[39] J.S. Park, W. Park, S.-j. Park, A.C. Larson, D.-H. Kim, K.-H. Park, Multimodal magnetic nanoclusters for gene delivery, directed migration, and tracking of stem cells, Adv. Funct. Mater. 27 (2017) 1700396.
[40] Y. He, Y. Nie, G. Cheng, L. Xie, Y. Shen, Z. Gu, Viral mimicking ternary polyplexes: a reduction-controlled hierarchical unpacking vector for gene delivery, Adv. Mater. 26 (2014) 1534–1540.
[41] H. Kim, S. Kim, S. Kang, Y. Song, S. Shin, S. Lee, M. Kang, S.H. Nam, Y. Lee, Ring opening metathesis polymerization of bicyclic α,β-unsaturated anhydrides for ready-to-be-grafted polymers having tailored pH-responsive degradability, Angew. Chem. Int. Ed. 57 (2018) 12468–12472.
[42] H. Tan, C.R. Chu, K.A. Payne, K.G. Marra, Injectable in situ forming biodegradable chitosan–hyaluronic acid based hydrogels for cartilage tissue engineering, Biomaterials 30 (2009) 2499–2506.
[43] L. Zhao, A. Kutikov, J. Shen, C. Duan, J. Song, G. Han, Stem cell labeling using polyethylenimine conjugated (α-NaYbF(4):Tm(3+))/CaF(2) upconversion nanoparticles, Theranostics 3 (2013) 249–257.
[44] K. Zhu, G. Liu, J. Hu, S. Liu, Near-infrared light-activated photochemical internalization of reduction-responsive polyprodrug vesicles for synergistic photodynamic therapy and chemotherapy, Biomacromolecules 18 (2017) 2571–2582.
[45] X. Wang, K. Liu, G. Yang, L. Cheng, L. He, Y. Liu, Y. Li, L. Guo, Z. Liu, Near-infrared light triggered photodynamic therapy in combination with gene therapy using upconversion nanoparticles for effective cancer cell killing, Nanoscale 6 (2014) 9198–9205.
[46] M.A. Jackson, T.A. Werfel, E.J. Curvino, F. Yu, T.E. Kavanaugh, S.M. Sarett, M.D. Dockery, K.V. Kilchrist, A.N. Jackson, T.D. Giorgio, C.L. Duvall, Zwitterionic nanocarrier surface Chemistry improves siRNA tumor delivery and silencing activity relative to polyethylene glycol, ACS Nano 11 (2017) 5680–5696.
[47] S. Daum, M.S.V. Reshetnikov, M. Sisa, T. Dumych, M.D. Lootsik, R. Bilyy, E. Bila, C. Janko, C. Alexiou, M. Herrmann, L. Sellner, A. Mokhir, Lysosome-targeting amplifiers of reactive oxygen species as anticancer prodrugs, Angew. Chem. Int. Ed. 56 (2017) 15545–15549.
[48] L. Tang, X. Yang, Q. Yin, K. Cai, H. Wang, I. Chaudhury, C. Yao, Q. Zhou, M. Kwon, J.A. Hartman, I.T. Dobrucki, L.W. Dobrucki, L.B. Borst, S. Lezmi, W.G. Helferich, A.L. Ferguson, T.M. Fan, J. Cheng, Investigating the optimal size of anticancer nanomedicine, PNAS 111 (2014) 15344–15349.
[49] R. Mo, Q. Sun, J. Xue, N. Li, W. Li, C. Zhang, Q. Ping, Multistage pH-responsive liposomes for mitochondrial-targeted anticancer drug delivery, Adv. Mater. 24 (2012) 3659–3665.
[50] H. Zhao, W. Hu, H. Ma, R. Jiang, Y. Tang, Y. Ji, X. Lu, B. Hou, W. Deng, W. Huang, Q. Fan, Photo-induced charge-variable conjugated polyelectrolyte brushes encapsulating upconversion nanoparticles for promoted siRNA release and collaborative photodynamic therapy under NIR light irradiation, Adv. Funct. Mater. 27 (2017) 1702592.
[51] Y. Wang, Y. Deng, H. Luo, A. Zhu, H. Ke, H. Yang, H. Chen, Light-responsive nanoparticles for highly efficient cytoplasmic delivery of anticancer agents, ACS Nano 11 (2017) 12134–12144.
[52] J. Liu, G. Yang, W. Zhu, Z. Dong, Y. Yang, Y. Chao, Z. Liu, Light-controlled drug release from singlet-oxygen sensitive nanoscale coordination polymers enabling cancer combination therapy, Biomaterials 146 (2017) 40–48.
[53] P. Li, H. Song, H. Zhang, P. Yang, C. Zhang, P. Huang, D. Kong, W. Wang, Engineering biodegradable guanidyl-decorated PEG-PCL nanoparticles as robust exogenous activators of DCs and antigen cross-presentation, Nanoscale 9 (2017) 13413–13418.
[54] S.J. Park, W. Park, K. Na, Tumor intracellular-environment responsive materials shielded nano-complexes for highly efficient light-triggered gene delivery without cargo gene damage, Adv. Funct. Mater. 25 (2015) 3472–3482.
[55] X. He, X. Wu, K. Wang, B. Shi, L. Hai, Methylene blue-encapsulated phosphonate-terminated silica nanoparticles for simultaneous in vivo imaging and photodynamic therapy, Biomaterials 30 (2009) 5601–5609.
[56] Y. Zhang, K. Ren, X. Zhang, Z. Chao, Y. Yang, D. Ye, Z. Dai, Y. Liu, H. Ju, Phototearable tape close-wrapped upconversion nanocapsules for near-infrared modulated efficient siRNA delivery and therapy, Biomaterials 163 (2018) 55–66.